FINAL
IN-02-CR
OCIT.
43901

Aerodynamic Requirements for BVI Noise Control

Final Report
NASA Grant NAG 2-844

Valana L. Wells
Arizona State University

April 1996

Chapter 1 Introduction

As a rotor blade moves through the air, it sheds vortices. These vortices shed along the length of the blade over time form the wake. The strongest vortices of the wake are those trailing from the tip of the blade. When a rotating blade system moves under certain operating conditions, each blade will impinge on the tip vortices shed by itself or other blades. This impingement is called a blade-vortex interaction, or BVI. Although the blade and trailing tip vortices interact with many different orientations, one of the two extremes, either parallel or perpendicular interaction, is usually modelled (see fig. 1). In a perpendicular interaction, the portion of the blade that is actually interacting with the travelling vortex at any given time is very small. A parallel interaction, however, has the largest concurrent interaction with the blade, as a result this case is given the most attention.

One of the most commonly studied occurrences of blade-vortex interactions is associated with low-speed descending rotorcraft flight. BVI occur when the tip vortices shed by the blades intersect the plane of the rotor. BVI cause local pressure changes over the blades which are responsible, in part, for the acoustic signature of the rotorcraft. The local pressure changes also cause vibrations which lead to fatigue of both the blades and the mechanical components driving the blades. If the pressure changes over the blades can be predicted and subsequently reduced, presumably these negative effects will also

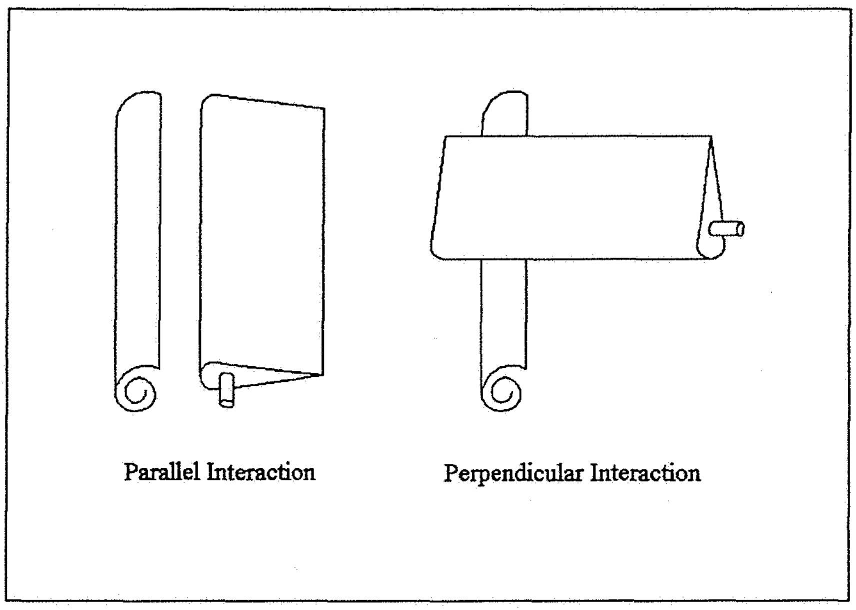

Figure 1: Parallel and Perpendicular Interactions

be reduced.

When rotorcraft operate in populated areas, their acoustic signatures are often cited as a source of annoyance for people in the surrounding area. This is because many of the operations near populated areas are in the low speed descending or maneuvering regimes. Reduction of rotorcraft noise is necessary before they become acceptable as a common form of city-center to city-center transportation. This noise reduction will not be possible until the effect of BVI can be predicted accurately enough so that methods to minimize them can be evaluated.

1.1 Previous Work

Previous work has been done in the prediction of two dimensional, parallel blade vortex interactions. Lee and Smith,[1] discuss the effect of vortex distortion on the aerodynamics of a blade section. The effect of a vortex a minimum distance away can be measured, but the actual dynamics of the vortex core are unknown. One option is to use a single point moving in the system as the travelling vortex - this is referred to as the point-vortex model. This model is not valid, however, if the vortex approaches a surface closely, because the velocities induced at the center of the vortex will be very large. Lee and Smith concede that using the point-vortex representation is valid as long as the vortex is not allowed to get too close to the airfoil. Wu *et al.*,[2] present a conformal mapping approach to the question of blade-vortex interaction in incompressible flow. They show that BVI produce rapid pressure changes at the leading edge of the airfoil. Yao,[3] shows the lift variations on an airfoil section as a vortex moves past, using a panel method for calculation. Yao presents comparisons between the panel method results and those of Wu *et al.*, Lee and Smith, and others. The effect of adding elasticity to the blade has been approached by Wells,[4]. The theoretical results presented by Wells show the importance of considering the aeroelastic characteristics of the blade and some of the problems associated with using trailing edge flaps to control rotor noise. Derham and

Oh,[5] present analytical data on the effect of blade elasticity on BVI. They conclude that aeroelastic considerations are especially important in studying sound in the low frequency range.

1.2 Present Work

An unsteady, constant potential panel code is developed from Green's identity, following the steps for developing the steady, constant source panel code presented by Moran,[6]. Unlike the code developed by Moran,[6], the unsteady code incorporates unsteady flow conditions and includes motion of the blade section. Constant potential panels model either four or five digit NACA designation airfoil blade sections in two dimensions. The potential at any point in the domain is calculated and used to determine characteristics of the airfoil section including the distribution of pressure coefficient, c_p, the lift coefficient, c_l, and the moment coefficient, c_m. Also looked at in this study are the effect of center of gravity placement and blade thickness. Some other things that can be studied using this code are changes in the blade characteristics, such as, blade stiffness and airfoil thickness, and the resulting lift and moments.

Chapter 2 Development

2.1 Original Panel Method

The basis for the current panel code is the two dimensional, steady, incompressible, irrotational blade element code developed by Moran,[6]. Figure 2 represents the modeled system, with a blade section placed inside a computational domain. The outside boundary of the domain is called the far-field. This is the set of points at which any perturbation in pressure or velocity due to the disturbances generated in the center of the domain are negligible. The domain is made a simply connected domain by the branch cut leading from the trailing edge to the far-field surface. This branch cut is used to numerically account for the jumps in velocity potential, φ, and velocity, $\nabla\varphi$, which occur across the trailing edge.

In the original code, constant source and vortex panels are used to model the surface of the blade. The velocity potentials, φ_{∞}, in the freestream, and the source potentials on the surface both satisfy Laplace's equation,

$$\nabla^2\varphi = 0 \tag{2.1}$$

Laplace's equation, 2.1, is used to produce a simplified version of Green's identity, which is valid for a simply connected domain,

$$\varphi_p = \int_s \left[(\hat{n} \cdot \nabla\varphi)\, G - \varphi(\hat{n} \cdot \nabla G) \right] dS \tag{2.2}$$

Where, G is the Green's function, or the fundamental solution for Laplace's equation. Equation, 2.2, can be used to solve for the potential at any point, p, in the domain. The integration surface, S, includes the airfoil surface, S_a, the wake "surface", S_w, and the far-field "surface", S_∞ (see fig. 2). The first term in Green's identity, $(\hat{n} \cdot \nabla\varphi)\, G$, represents the potential at point p due to the source distribution on the segment, dS. The second term, $\varphi(\hat{n} \cdot \nabla G)$, is defined by Moran,[6] as the rate of change of φ in the direction of $\hat{n}$ on the segment, dS. The far-field assumptions are separated by integrating over S_∞. Completing this integral results in,

$$\varphi_\infty = V_\infty(x \cos\alpha + y \sin\alpha)$$

where α is the angle of attack of the airfoil. After integrating over the far-field terms, Green's identity leaves a total potential of,

$$\varphi_p = V_\infty(x_p \cos\alpha + y_p \sin\alpha) + \int_s \left[(\hat{n} \cdot \nabla\varphi)\, G - \varphi(\hat{n} \cdot \nabla G) \right] dS \tag{2.3}$$

where S is now S_a and S_w. Using the idea that the influences of source and vortex panels can be described by the terms in Green's identity, equation 2.4 can be rewritten as

$$\varphi_p = V_\infty(x_p \cos\alpha + y_p \sin\alpha) + \int_s \sigma G dS - \int_s \gamma \int (\nabla G \cdot \hat{n}) dS \tag{2.4}$$

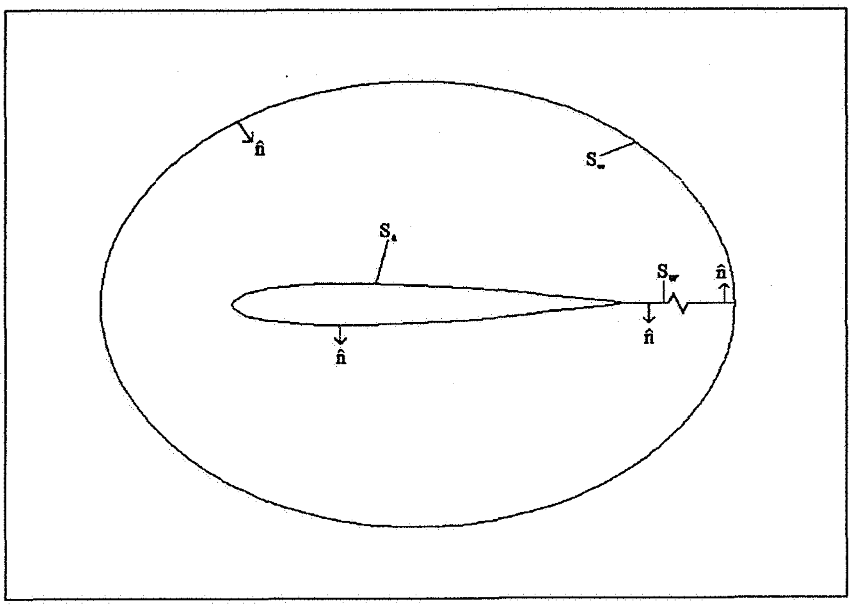

Figure 2: Computational Domain

where σ is the distributed source strength, and γ is the distributed vortex strength. This equation can be converted to a statement of zero normal velocity by taking $\hat{n} \cdot \nabla \varphi_p = 0$ at the surface. The resulting equation is then discretized and solved for the unknown source and vortex strengths. The above procedure, originally proposed by Smith and Hess,[7], describes a standard procedure for developing a panel method. However, when unsteady pressures are to be computed, it is more convenient to solve for the potentials directly. Therefore, it was decided to utilize a constant-potential panel method for the current study.

2.2 Constant Potential Panel Method

If the panels representing the blade element are represented as constant potential surfaces, the constant source code presented by Moran, [6] becomes a constant potential code. If the blade element is kept stationary with no flow through the surface, then the $\hat{n} \cdot \nabla \varphi$ term in Green's Identity, eqn. 2.3, goes to zero. The $\varphi(\hat{n} \cdot \nabla G)$ term can be simplified by integrating over the wake and the airfoil separately. Moran,[6] represents circulation numerically using a steady Kutta condition. The Kutta condition in steady flow requires that the aft stagnation point lie at the trailing edge. The physical manifestation of the Kutta condition is that the air flow leaves the trailing edge smoothly. As flow leaves the trailing edge, it assumes the φ value of the surface which it leaves. This means that the potential of the flow leaving the trailing edge, and forming the wake, has different values for the upper and lower surfaces. Thus, following from the steady Kutta condition, circulation is defined as,

$$\Gamma = \varphi_N - \varphi_1 \tag{2.5}$$

where the subscript $_1$ is the farthest aft panel on the bottom surface, and $_N$ is the trailing edge panel on the top surface. Finally, equation 2.3, the equation for the potential at any point in the domain becomes,

$$\varphi_p = V_\infty(x_p \cos\alpha + y_p \sin\alpha) - \int_{s_a} \varphi(\hat{n} \cdot \nabla G) dS - \Gamma \int_{s_w} \hat{n} \cdot \nabla G dS \qquad (2.6)$$

Evaluating equation 2.6 numerically at the midpoint of each of the panels that make up the discretized airfoil results in

$$\varphi_i = V_\infty(\bar{x}_i \cos\alpha + \bar{y}_i \sin\alpha) - \sum_{j=1}^{N} \varphi_j \int_{panelj} \hat{n} \cdot \nabla G dS - \Gamma \int_{s_w} \hat{n} \cdot \nabla \varphi dS \qquad (2.7)$$

for each i^{th} panel. Once the potential at each point has been determined, Bernoulli's equation,

$$c_p = 1 - v_{\text{tang}}^2 \qquad (2.8)$$

is used to determine the pressure coefficient for each panel of the blade. The c_p is then be used to calculate c_l and c_m for the entire blade

This numerical model is commonly used in studying steady, incompressible, irrotational flow. For the current study, modifications were made to the code to allow for airfoil movement and to incorporate a travelling vortex.

2.3 Current Panel Method

The current panel code modifies Moran's code,[6] by taking into account aeroelastic blade movement, a travelling vortex, and by accommodating the resulting unsteady wake. Figure 3 depicts a simplified view of the current problem. Allowing aeroelastic movement of the blade means that the normal velocity of the air at the surface of the blade is no

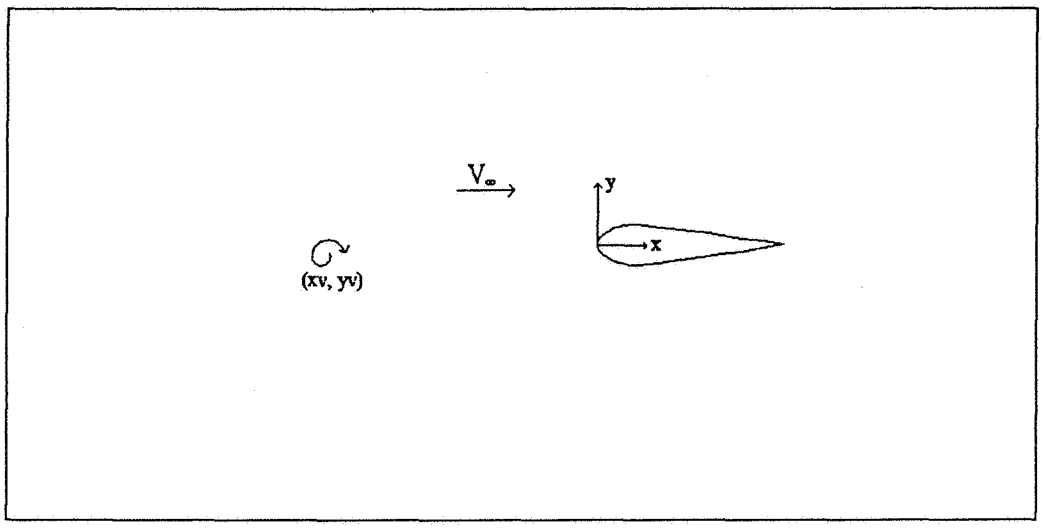

Figure 3: Unsteady Problem

longer zero, instead it is equal in magnitude and direction to the movement of the blade at each panel. This means that the first term in Green's identity, see eqn. 2.3, can not be eliminated over the airfoil as it was for the steady code. The travelling vortex is treated as the potential due to a discrete point-vortex of known strength and starting position. Modelling the wake presents a more complicated problem than that of adding a travelling vortex. The wake can not be represented as a single panel as it was in the steady case because the vorticity of the airfoil is no longer constant. Kelvin's vorticity conservation law states that the total vorticity of the system must remain constant, whether the system is steady or unsteady. In an unsteady problem the potential of the surface panels change accordingly at each time step. Circulation, which is still defined as the difference in potential at the trailing edge, see eqn. 2.5, must change at each time step to compensate for the changing vorticity of the airfoil and to keep the total vorticity of the system constant. Mathematically, this means that the potential jump across the wake can not be removed from the second term in the integral in equation 2.3, as was done in equation 2.7. The potential at each point in the domain, including all of the unsteady conditions, becomes,

$$\varphi_p = V_\infty(x_p \cos\alpha + y_p \sin\alpha) + \varphi_v - \int_{s_{a+s_w}} (\hat{n}\cdot\nabla G)\,\varphi dS + \int_{s_a} G(\hat{n}\cdot\nabla\varphi) dS \quad (2.9)$$

where φ_v represents the potential due to the travelling vortex. This equation, along with the aeroelastic equations of motion, describes the problem that is being modeled.

2.3.1 Aeroelastic Equations

Wells,[4] provides the basis of the aeroelastic movement of the blade element. Figure 4 presents the aeroelastic system model. This is the simplest aeroelastic model, with one spring for plunging motion, and one for pitching. Both springs are anchored at the elastic axis, x_{ea}. The elastic axis is commonly located at one quarter of the distance from the leading edge to the trailing edge, or at the quarter-chord. The quarter-chord is also often where the center of gravity, x_{cg} is placed. The governing equations are which are force and moment equations.

$$\bar{m}\ddot{z} - l + k_z z - S_\alpha\ddot{\alpha} = k_z z_o \quad (2.10)$$

and

$$I_{ea}\ddot{\alpha} - m_{ea} + k_\alpha\alpha - S_\alpha\ddot{z} = k_\alpha\alpha_o \quad (2.11)$$

Where $\bar{m}$ is the mass per unit length based on the properties for Aluminum; I_{ea} is the mass moment of inertia per unit length, which has been solved for a generic box-beam; l and m_{ea} are the aerodynamic force and moment on the airfoil; S_α is the term which couples the translational and rotational energies when the elastic axis, x_{ea}, and the center of gravity, x_{cg}, are not collocated, (if they are at the same point then S_α is zero); α_o and z_o are the initial angle of attack and y-axis displacement; α and z are the aeroelastic unknowns, and k_z and k_α are the effective spring constants in flapping and torsion. The governing equations, 2.10 and 2.11, are a pair of coupled differential equations, and can be manipulated into a nondimensional matrix equation,

$$\dot{\mathrm{x}} = A\mathrm{x} + f(\mathrm{x}, t) \tag{2.12}$$

$$A = \frac{1}{1-\bar{S}^2}\begin{bmatrix} 0 & 0 & -\kappa_z & -\bar{S}\kappa_\alpha \\ 0 & 0 & -\bar{S}\kappa_z & -\kappa_\alpha \\ (1-\bar{S}^2) & 0 & 0 & 0 \\ 0 & (1-\bar{S}^2) & 0 & 0 \end{bmatrix} \tag{2.13}$$

$$f(x,t) = \frac{1}{1-\bar{S}^2}\begin{Bmatrix} \bar{m}c_\ell + \bar{S}\left(\bar{I}c_m + \kappa_\alpha\alpha_o\right) + \kappa_z z_o \\ \bar{I}c_m + \bar{S}\left(\bar{m}c_\ell + \kappa_z z_o\right) + \kappa_\alpha\alpha_o \\ 0 \\ 0 \end{Bmatrix}$$

where $\mathrm{x} = (\dot{z}, \dot{\alpha}, z, \alpha)^T$, A contains the nondimensional spring constants and inertias, and $f(x,t)$ contains the aerodynamics. This matrix equation is solved with a partially

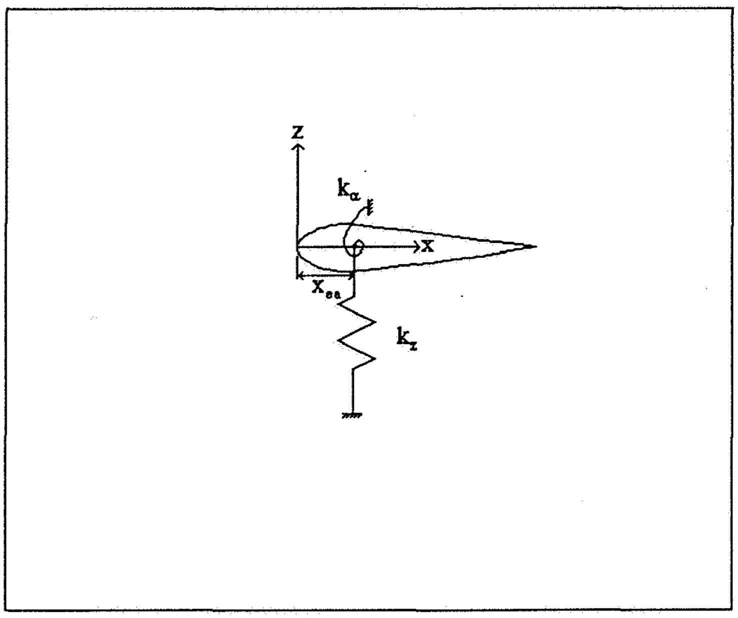

Figure 4: Aeroelasticity Model

implicit Euler finite difference method,

$$\mathrm{x}^n = (I - \Delta t A)^{-1}(\mathrm{x}^{n-1} + \Delta t f^{n-1}) \tag{2.14}$$

where the superscript refers to the time step, n being the current time step, and $n-1$ the previous step, and Δt is the size of the time step.

2.3.2 Kutta Condition

One of the most interesting aspects of an unsteady, inviscid flow model is the problem of how to model the flow at the trailing edge. In steady flow, the Kutta condition requires that flow leave the trailing edge of the airfoil smoothly. This implies that the stagnation point needs to lie at the trailing edge, and that the wake will extend from there. In a model incorporating a travelling vortex, however, the flow is no longer steady, regardless of whether the blade is stationary. The steady Kutta condition is, in general, invalid in the unsteady case because the flow no longer necessarily leaves the trailing edge smoothly. Instead, for unsteady flow the Kutta condition states that the pressure difference between the upper and lower trailing edge surfaces be zero,

$$\triangle c_p = -2\frac{\partial \triangle \varphi}{\partial t} + \left(v_{lower}^2 - v_{upper}^2\right) = 0 \tag{2.15}$$

In the present code the unsteady Kutta condition is satisfied indirectly. First, the potential difference across the wake is extrapolated in time from the upper and lower surfaces of the trailing edge using an equation derived from the unsteady Kutta condition 2.15,

$$\triangle \varphi^n = \triangle \varphi^{n-1} + \frac{\triangle t}{2}\left(v_{lower}^2 - v_{upper}^2\right)^{n-1} \tag{2.16}$$

Then $\triangle c_p$ is checked to see if it falls within a prescribed limit, if it does not, the equation is iterated for a value of $\triangle \varphi^n$ that results in a $\triangle c_p$that satisfies the prescribed limit. Thus the unsteady Kutta condition is satisfied indirectly. In the first time step this extrapolation is not used, because the system undergoes an impulsive start, so $\triangle \varphi$ is set to zero for the first step.

It would likely be more accurate to iterate on the location of the first panel in the wake rather than the potential difference across the first panel. This would be a more rigorous solution to the unsteady Kutta condition because it is more likely to mimic the process that actually takes place in the physical realm. Unfortunately, iterating on the position of the first wake panel would require prohibitive amounts of computer time and memory because it means moving the panel and then re-calculating the influence it had on every other point in the system. Setting the position of the first panel and iterating on the potential difference over it seems less realistic but computationally is much more feasible. Once the potential for that panel has been calculated, it is held constant in subsequent time steps, and the panel locations are allowed to move according to the influence of the rest of the system. In running the code it has been found that the original extrapolation proves, in most cases, to be an adequate estimate of the new wake panel strength.

2.4 Numerical Implementation

2.4.1 Discretization of the Problem

Much of the numerical implementation of eqn. 2.9 is straight forward. The influence of the freestream, $V_\infty(x_p \cos\alpha + y_p \sin\alpha)$, is calculated using the angle of attack of the airfoil, α, and the nondimensional freestream velocity. The potential due to the travelling vortex is defined as,

$$\varphi_v = -\frac{\Gamma}{2\pi}\theta \tag{2.17}$$

where the strength of the vortex, Γ, is given; and θ is the angle from the horizontal at the vortex to the blade element segment being evaluated and is calculated for every segment at each time step. For the last two terms of eqn. 2.9, the definition of a unit source potential in two dimensions can be used to simplify the calculations,

$$G = \frac{1}{2\pi} \ln r \tag{2.18}$$

where r is the distance between the point of interest and the point it is influencing. Using this definition, the influence of a particular potential panel is calculated as a function of distance, a parameter that is easily determined. The $\int_{s_a+s_w} (\hat{n} \cdot \nabla G)\, \varphi dS$ term of eqn. 2.9 encompasses the effect that the other blade element panels and the wake have on each particular panel. In unsteady flow, the vorticity around the airfoil changes at every time step. In order to conserve vorticity according to Kelvin's law, the vorticity of the wake at each time step must change accordingly in order to have a strength equal and opposite that of the airfoil. This is modeled by extending the wake at each time step with a "panel" shed from the trailing edge. The effect of these wake "panels" on a particular airfoil panel is mathematically similar to the effect due to other airfoil panels. The dimensionless numerical potential equation used in the code is,

$$\begin{aligned} \varphi_p \;=\;& x_p \cos\alpha + y_p \sin\alpha - \frac{\Gamma}{2\pi}\theta - \sum_{j=1}^{N} \left(\frac{\partial \varphi}{\partial n}\right)_{panelj} \int_{panelj} \frac{1}{2\pi} \ln r_{pj} dS \\ &+ \sum_{j=1}^{N} \varphi_{panelj} \int_{panelj} \frac{\partial}{\partial n}\left(\frac{1}{2\pi}\ln r_{pj}\right) dS + \sum_{k=1}^{M} \triangle\varphi_k \int_{panelk} \frac{\partial}{\partial n}\left(\frac{1}{2\pi}\ln r_{pk}\right) dS \end{aligned} \tag{2.19}$$

where the subscript p refers to the point of interest; j, to each airfoil panel; and k, to each wake panel. The nondimensionalization process is standard, the velocities are nondimensionalized by the freestream velocity, r by the chord, t by V_∞/c, and Γ by the freestream velocity times the chord. The importance of this equation is that it shows that the unknowns are the φ_j's on each airfoil panel. At each time step, the influence on a panel due to every other potential source in the domain is calculated and these contributions are summed. This is accomplished mathematically by solving an $N \times N$ matrix for the N unknown airfoil panel potentials.

Once the potentials have been calculated for a particular time step, the pressure at each panel on the airfoil at that time step is determined using an unsteady, dimensionless form of Bernoulli's equation

$$c_p = 1 - v^2 + 2\frac{\partial\varphi}{\partial t} \tag{2.20}$$

where v is the total fluid velocity. The pressures at all of the panels are then used to determine the unsteady lift and moment for the airfoil section.

2.4.2 Numerical Procedure

Figure 5 is a flow chart which summarizes the steps followed by the program. The code begins with an impulsive start. First the dynamics matrix is decomposed because it does not depend on time. Next, node points are placed to define the panels used to approximate the airfoil. As the time loop begins, the travelling vortex is placed in its initial position which has been read into the program. In subsequent steps, the travelling vortex is moved to its new position and a constant potential panel is shed from the trailing edge. At the same time the wake panels shed at previous time steps are moved to their new locations which are calculated by incorporating the influence of everything else in the domain. The position of the first wake panel is estimated using eqn. 2.16. With this assumed position, the potential matrix is inverted and the strength of the potential on each airfoil panel is computed. The panel potentials are then used to calculate the c_p value at each node. The c_p values are used to determine c_l and c_m for the airfoil section at each time step. At this point, if the $\triangle c_p$ of the farthest aft panels on the upper and the lower surfaces do not fall within the specified tolerance for the unsteady Kutta condition, then the value of φ for the first wake panel is iterated on. If φ is iterated on, the potential matrix is solved again, the c_p's are recalculated, c_l and c_m are computed again, and the unsteady Kutta condition is re-checked. Once the unsteady Kutta condition is satisfied, the dynamics matrix is solved to set the airfoil in its new position for the next time step. The code was run on a Sun Workstation at Arizona State University. A typical computational time was on the order of an hour.

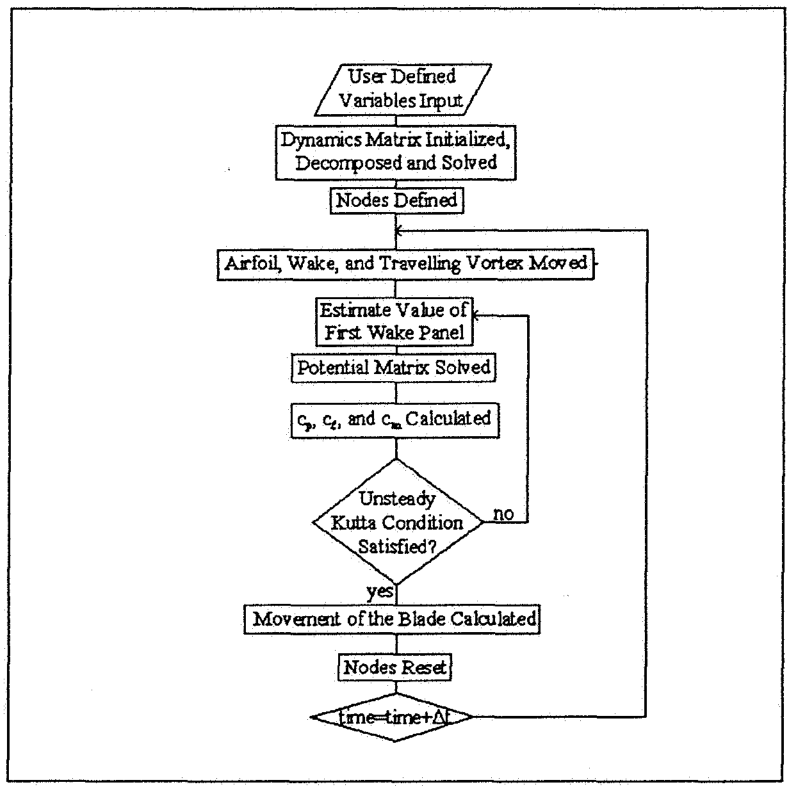

Figure 5: Program Flow Chart

Chapter 3 Results

3.1 Validation

3.1.1 Impulsive Start

The first step in the validation process was to check that the impulsive start of the system was correctly incorporated into the code, and did not have long term effects on the calculations. In order to validate the impulsive start, a NACA 0012 airfoil section was kept motionless and the travelling vortex's strength was set to zero. The most important characteristic of this case is the roll-up of the wake as it moves away from the airfoil. This signifies that the first vortices shed are the strongest, and that their strength is negative, as is expected for an airfoil with a positive angle of attack. The behavior of the wake, with one roll at the end, also indicates that the vortex strengths are diminishing with time.

Also compared for the impulsive start case, was the ratio of the lift at each time step divided by the lift at infinity, or steady-state. Figure 7 depicts the lift ratio variation. In the impulsive start case the constant potential panels suddenly gain initial values in a very small time, this means that the lift ratio starts at infinity. At the next time step, the ratio drops to one-half of the lift at steady-state. Then, as the strongest trailing edge vortices move away from the airfoil, the ratio slowly approaches one. The results from the current code follow this trend and show excellent agreement with the theoretical results for the impulsive start of a flat plate as given by Wagner, [8]. From this, it can be concluded that the effects of the impulsive start of the system become negligible very quickly.

3.1.2 Harmonic Plunging

The next step in the validation process was to compare the results of how moving the blade in a prescribed plunging motion affected the movement of the wake. A NACA 0015 airfoil section was set at an angle of attack, α, of zero degrees and then moved in a plunging motion prescribed by,

$$z(t) = z_{\max} \sin(2kt) \tag{3.1}$$

where $z_{\max}$ is the dimensionless plunging amplitude and k is the reduced frequency equal to $\omega c/2V_{\infty}$. The first trial was run using $z_{\max} = 0.018$ and $k = 2.15$, and the same case was also run for a reduced frequency of $k = 8.5$. The wake behind a heaving airfoil exhibits rolling tendencies due to the strength of the shed vortices and the fluctuation of the signs of the strengths over time. Figure 8 shows the wake formed using $k = 2.15$. Clusters of vortices can be seen forming at the points in the wake where the vortices change sign. At these points, the vortices begin to roll around each other. The wake formed by an airfoil plunging at a reduced frequency of $k = 8.5$ is made up of stronger vortices due to the rapid movement of the blade, this is shown in figure 9. The results from these two cases were compared with those of Giesing, [9], and Kim and Mook,

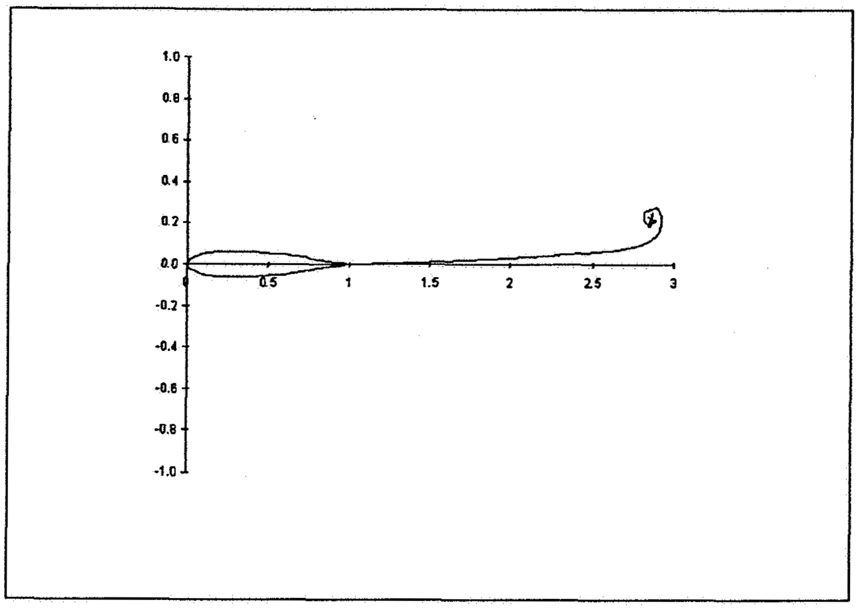

Figure 6: Impulsive Start Showing Wake Roll Up for a NACA 0012 Airfoil at $\alpha = 5°$

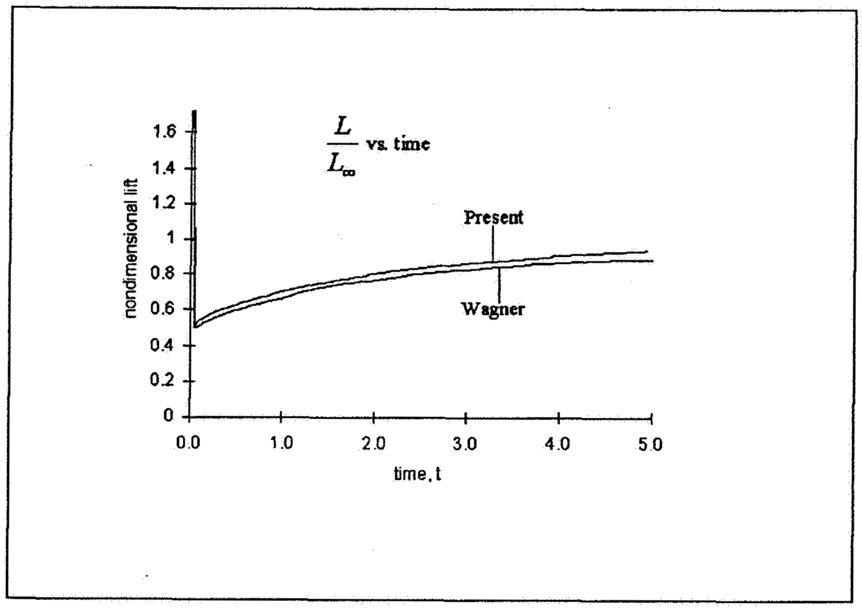

Figure 7: Lift Variation After an Impulsive Start for a NACA 0012 Airfoil at $\alpha = 5°$

[10]; the wakes look almost identical.

Another check of the effect of the plunging motion of the blade on the wake, was against the theoretical change in section lift, as described using Theodorsen's lift deficiency function. Katz and Plotkin,[8] state that the most important aspect of Theodorsen's function is that it succinctly describes the basic unsteady effects on the system. The same two cases were run for c_l comparison as were used in the wake comparisons, $\alpha = 0$, $z_{max} = 0.018$, and $k = 2.15$ or 8.5. The results of comparing section lift changes for an airfoil plunging at reduced frequencies of 2.15 and 8.5 are shown in figures 10 and 11. The reason for the differences in amplitude and phase between the case studied by Theodorsen and the present study is that Theodorsen used a flat plate approximation, so the airfoil in that case has no thickness. The sharp drop at the first time step in the results collected from the present study is due to the impulsive start of the system. Figure 12 shows the effect on the maximum c_l obtained by an airfoil section plunging at a reduced frequency of 8.5, using a $z_{\max}$ of 0.2. Using a second order curve fit to extrapolate the data illustrates the effect of thickness on maximum c_l.

Figure 13 shows the moment coefficient comparison for a NACA 0015 airfoil section. Theodorsen's lift deficiency function was used to validate the moment calculation part of the unsteady code, using $\alpha = 0$, $z_{\max} = 0.018$, and $k = 2.15$. The results show the same small differences in magnitude and phase that are apparent in the c_l comparisons, and the large amplitudes apparent at the leading edge are due to the impulsive start. The effect

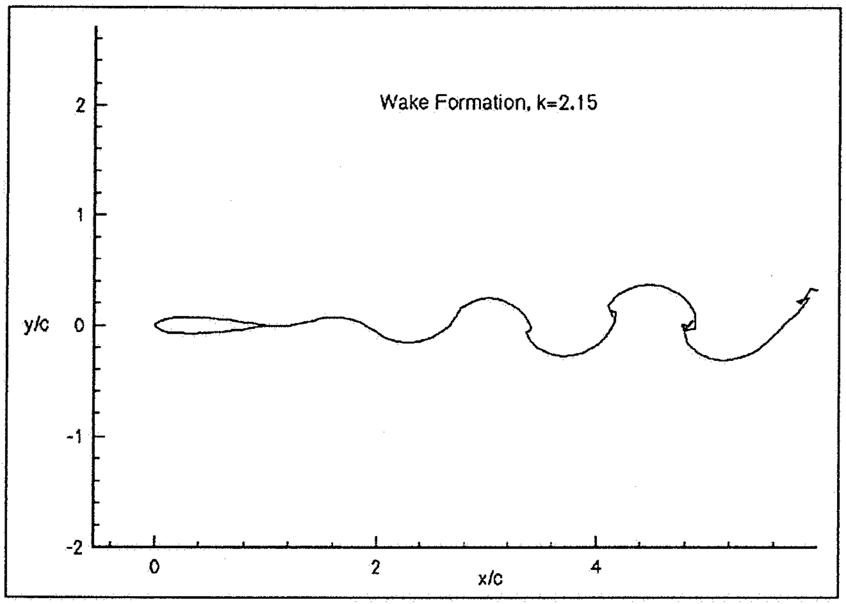

Figure 8: Wake Formation for a NACA 0015 Airfoil Plunging at $k = 2.15$ with $z_{\max} = 0.018$

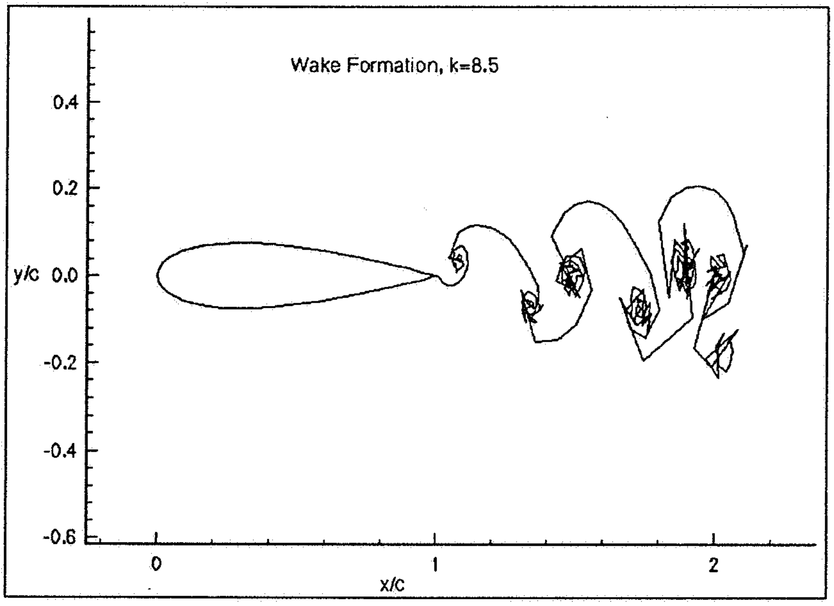

Figure 9: Wake Formation for a NACA 0015 Airfoil Plunging at $k = 8.5$ with $z_{\max} = 0.018$

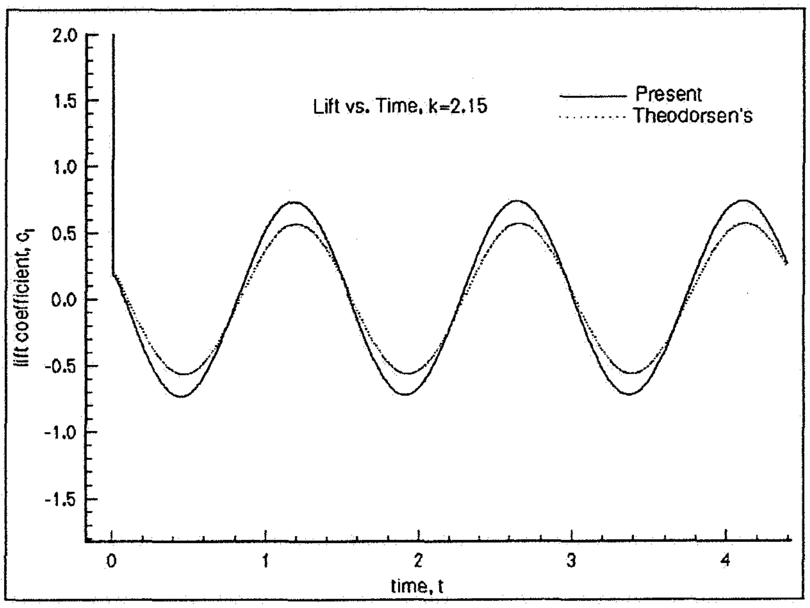

Figure 10: c_ℓ Comparison of a NACA 0015 Airfoil with Theodorsen's Exact Solution for a Flat Plate, $k = 2.15$, $z_{\text{max}} = 0.018$

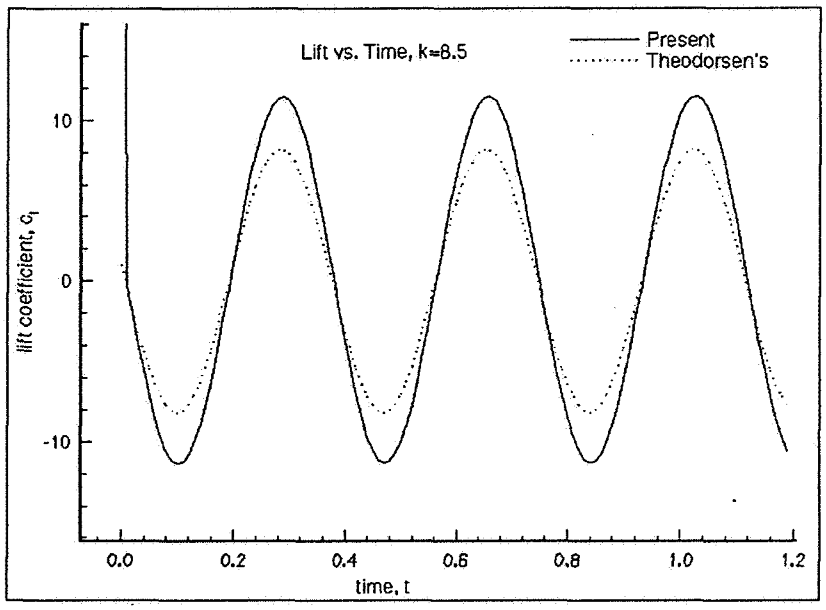

Figure 11: c_ℓ Comparison of a NACA 0015 Airfoil with Theodorsen's Exact Solution for a Flate Plate, $k = 8.5$, $z_{\text{max}} = 0.018$

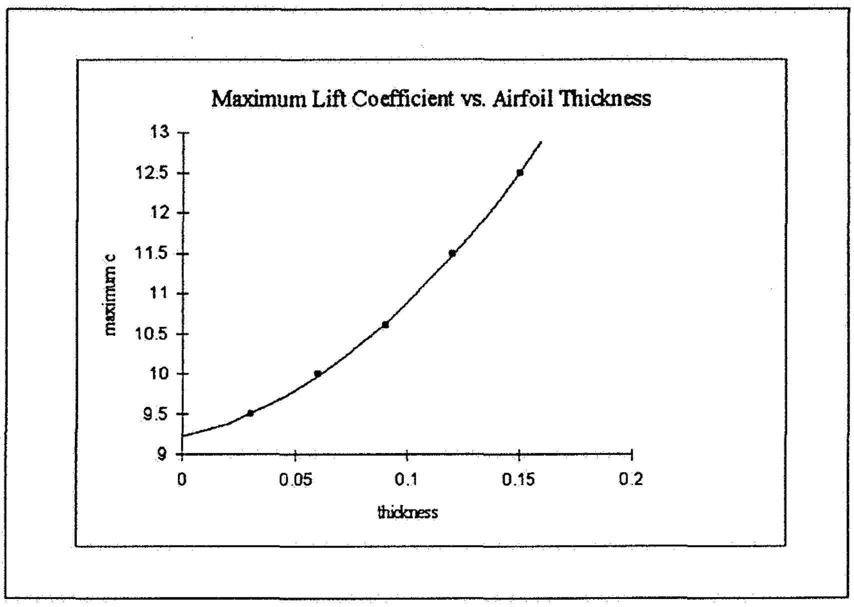

Figure 12: Variation of c_ℓ with Airfoil Section Thickness

of thickness on the magnitude and phase differences can be seen by comparing figure 13 with figure 14, which plots Theodorsen's function and results from the current code for a NACA 0003 airfoil. The differences due to airfoil thickness have all but disappeared.

3.1.3 Vortex Interaction with a Stationary Blade

Before adding a travelling vortex to the computational domain, the effect of the time step size was examined. With 82 panels representing the airfoil section, four trials were made letting a travelling vortex, with a strength of $\Gamma = 0.2$, move past a rigid airfoil. Data was collected using nondimensional time steps of $\Delta t = 0.1, 0.05, 0.025$ and 0.0125 as shown in fig. 15. The three sets of data show that, at the leading and trailing edges, the solution is still converging in time. For most of the c_l curve the time step does not

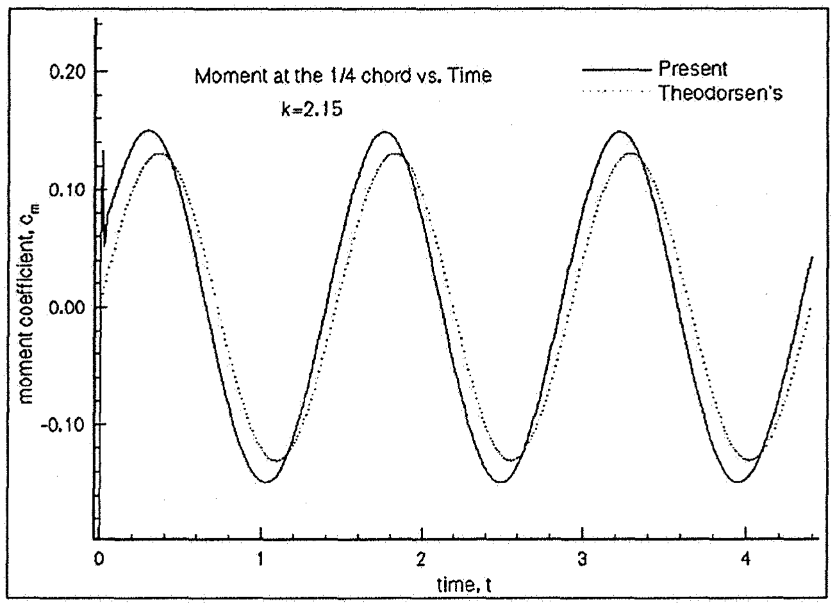

Figure 13: c_m Comparison of NACA 0015 Airfoil with Theodorsen's Exact Solution for a Flate Plate, $k = 2.15$, $z_{\max} = 0.018$

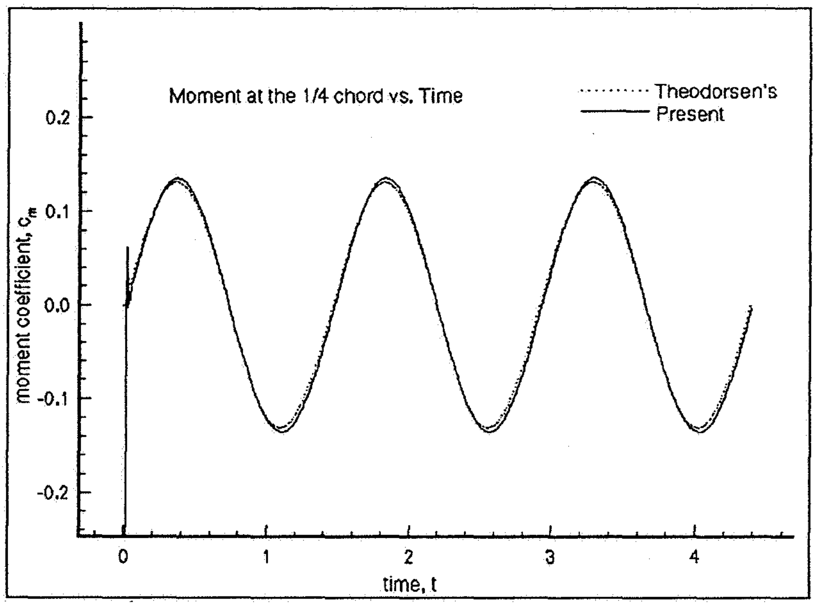

Figure 14: c_m Comparison of NACA 0003 Airfoil with Theodorsen's Exact Solution for a Flate Plate, $k = 2.15$, $z_{\max} = 0.018$

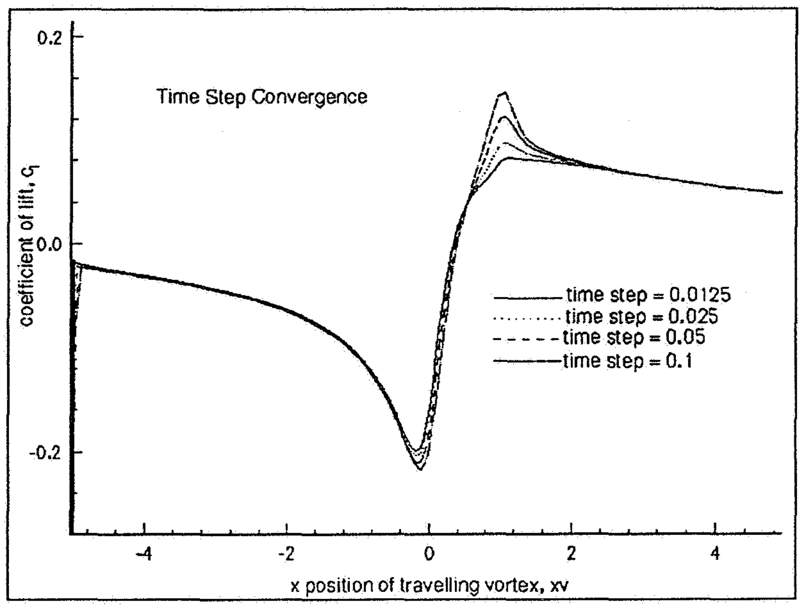

Figure 15: Effect of Time Step on c_ℓ Convergence for a NACA 0012 Airfoil Interacting with a Vortex, $\Gamma = 0.2$

have a significant effect, because the strongest interactions are confined to the leading and trailing edges. As the time step is divided in half, the computational time more than doubles. This means that the benefits of using a smaller time step for more accurate results must be weighed against the need for computational efficiency. To maximize accuracy and minimize computational time, a simple routine was added to allow an initial time step to be used until the travelling vortex is "close" to the airfoil, then the time step is cut in half. After the travelling vortex has passed the airfoil, the time step is reset to its initial value.

In order to validate the effect of the travelling vortex on the rotor blade, the blade was fixed in place and a travelling vortex, with $\Gamma = 0.2$, released six chord lengths in

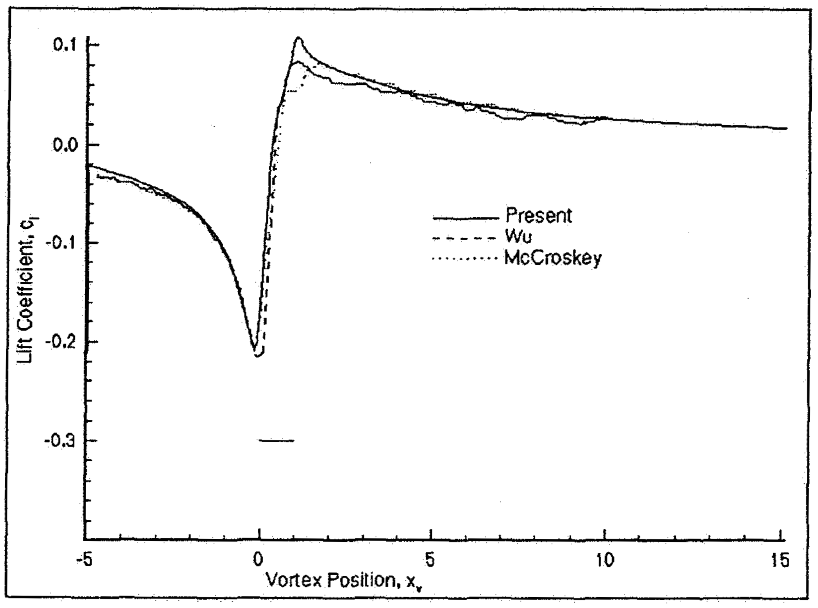

Figure 16: Comparison of c_ℓ Curves for a NACA 0012 Airfoil Interacting with a Vortex, $\Gamma = 0.2$

front of the blade and .26 chord lengths below it. Using a time step of 0.05, the variation of the airfoil lift coefficient as the travelling vortex moved by was compared with the variations computed by Wu et al.,[2] and McCroskey,[11]. The results of this comparison are shown in figure 16. The most noticeable differences occur at the trailing edge of the airfoil, little difference is seen elsewhere. This is expected because there are different methods of treating the conditions at the trailing edge.

3.2 Dynamic Results

3.2.1 Addition of Aeroelastic Springs

Once the code had been validated, comparisons were made between the results obtained including aeroelastic movement and those without it using a travelling vortex with nondimensional strength, $\Gamma = 0.5$. It is apparent from figures 17 and 18 that the addition of the aeroelastic springs of the blade has a distinct influence on the predicted values for the moment and lift coefficients, c_m and c_l. Once the vortex has passed the airfoil, its effect takes a while to damp out, causing oscillations in both the lift and moment coefficients. Figure 19 shows the effect on the c_l curve of decreasing the strength of the vortex to $\Gamma = 0.2$. While the magnitudes of the peak values have been lessened, the overall characteristics remain the same. Also affected by the addition of the aeroelastic springs is the path of the travelling vortex, fig. 20. This effect would be especially important when considering a vortex moving past more than one blade. Another parameter which is affected by adding springs is the change in angle of attack of the blade section as the vortex moves past. This is illustrated in figure 21. Although the magnitude of the oscillations is small relative to parameters such as c_l and c_m in figures 18 and 17, it will still produce added unsteady loading forces on the blade.

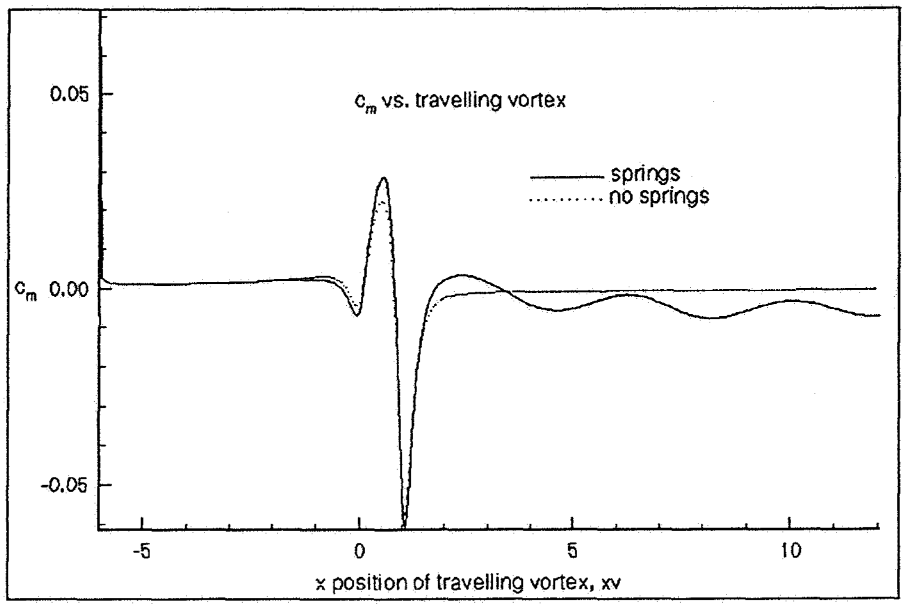

Figure 17: Effect of Aerodynamic Motion on c_m for a NACA 0012 Airfoil Interacting with a Vortex, $\Gamma = 0.5$

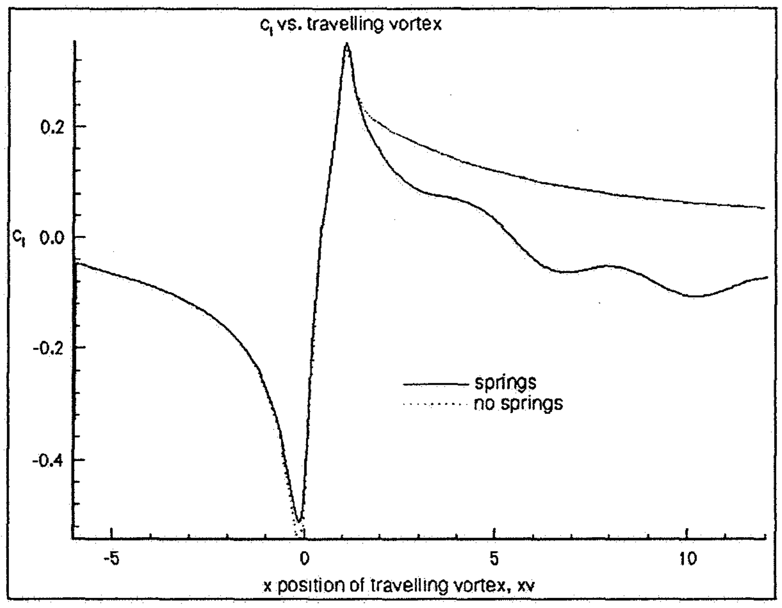

Figure 18: Effect of Aerodynamic Motion on c_ℓ for a NACA 0012 Airfoil Interacting with a Vortex, $\Gamma = 0.5$

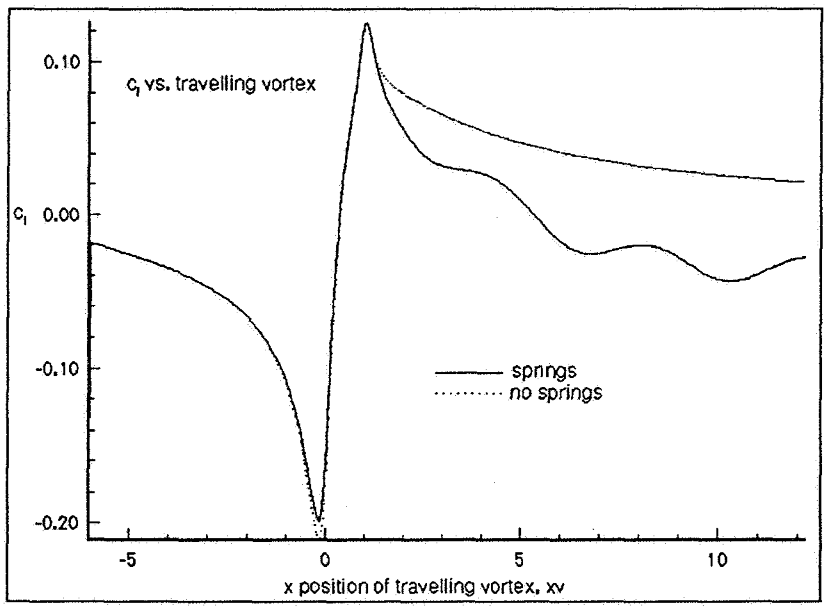

Figure 19: Effect of Aerodynamic Motion on c_ℓ for a NACA 0012 Airfoil Interacting with a Vortex, $\Gamma = 0.2$

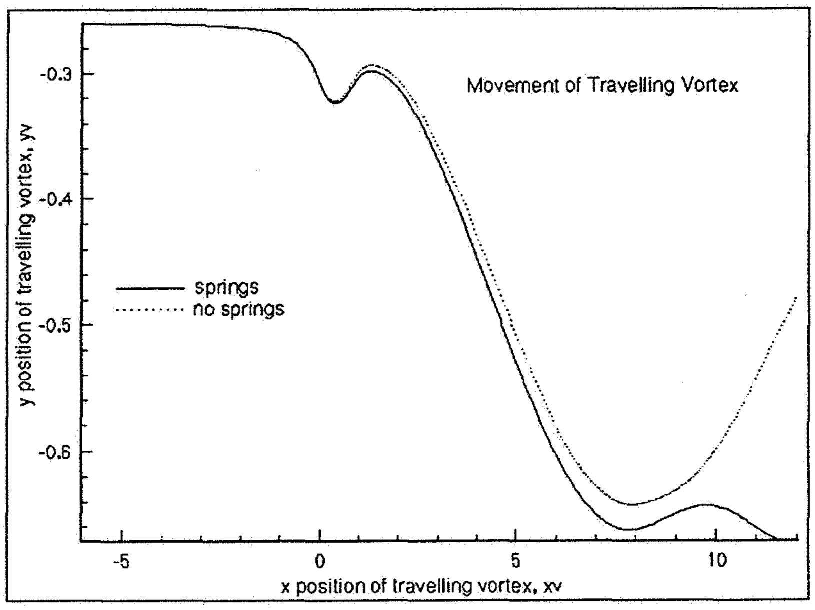

Figure 20: Effect of Aerodynamic Motion of a NACA 0012 on the Path of the Vortex, $\Gamma = 0.5$

3.2.2 Movement of the center of gravity

Often, rotorblades do not have their center of gravity at exactly the elastic axis. This can cause the blade to react in a somewhat different manner than that predicted by a rigid blade model, or even a simply aeroelastic model. If the center of gravity is not at the elastic axis, then the S_α terms from equations 2.10 and 2.11 are no longer zero. Figures 22 and 23 compare the effect of shifting the center of gravity $.05c$ in front of the elastic axis on c_ℓ and c_m. The shift of the center of gravity is also apparent in the basic movements of the blade, the angle of attack and y deflections. Figures 24 and 25 show angle of attack and y-deflection for the aeroelastic blade sections with the center of gravity at $0.2c$ and $0.25c$. The airfoil sections experience larger amplitude oscillations

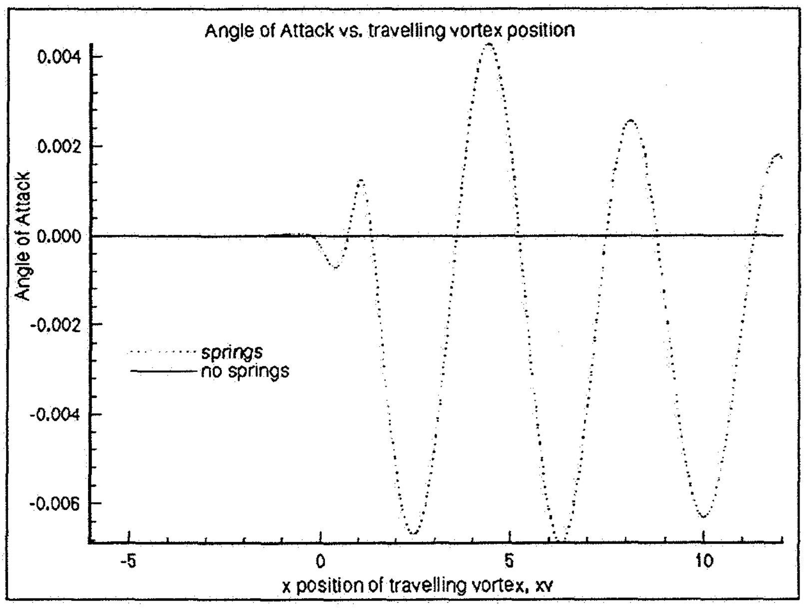

Figure 21: Effect of Aerodynamic Motion on Angle of Attack for a NACA 0012 Airfoil Interacting with a Vortex, $\Gamma = 0.5$

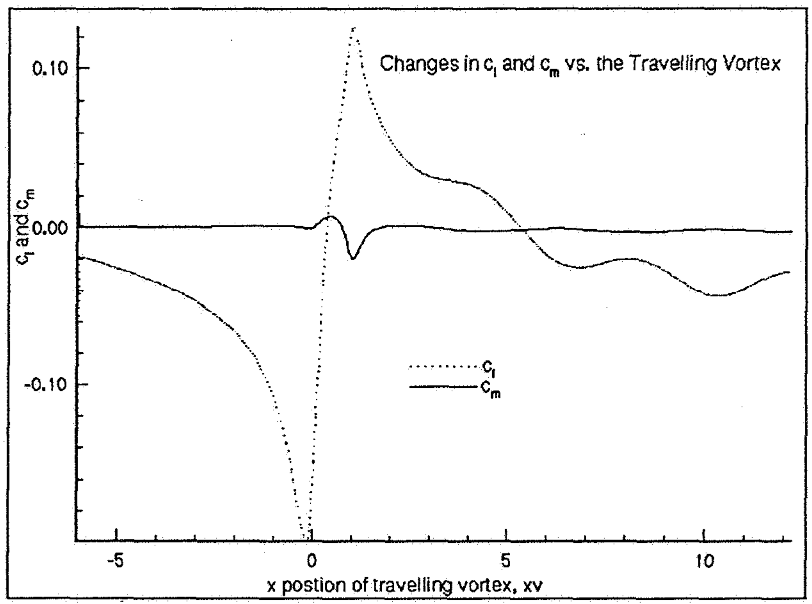

Figure 22: c_ℓ and c_m for a NACA 0012 Airfoil with the c.g. located at $0.25c$ Interacting with a Vortex, $\Gamma = 0.2$

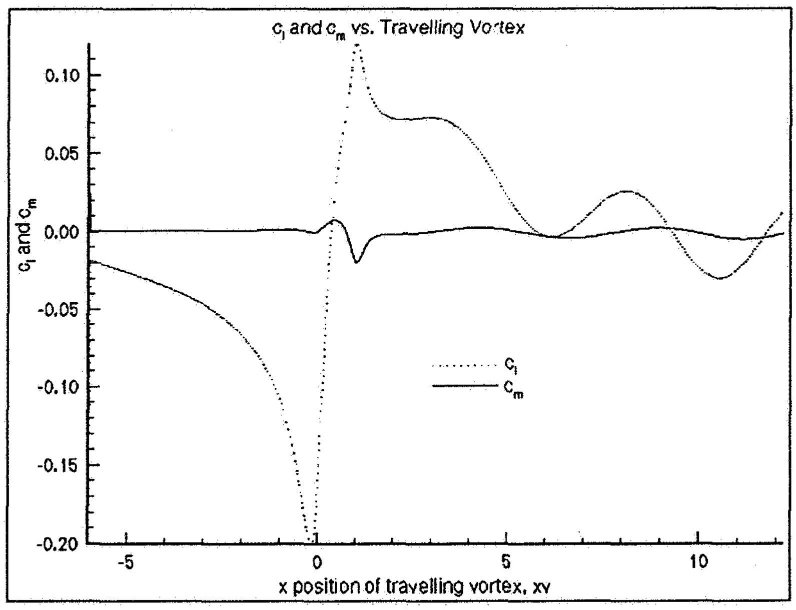

Figure 23: c_ℓ and c_m for a NACA 0012 Airfoil with the c.g. located at $0.2c$ Interacting with a Vortex, $\Gamma = 0.2$

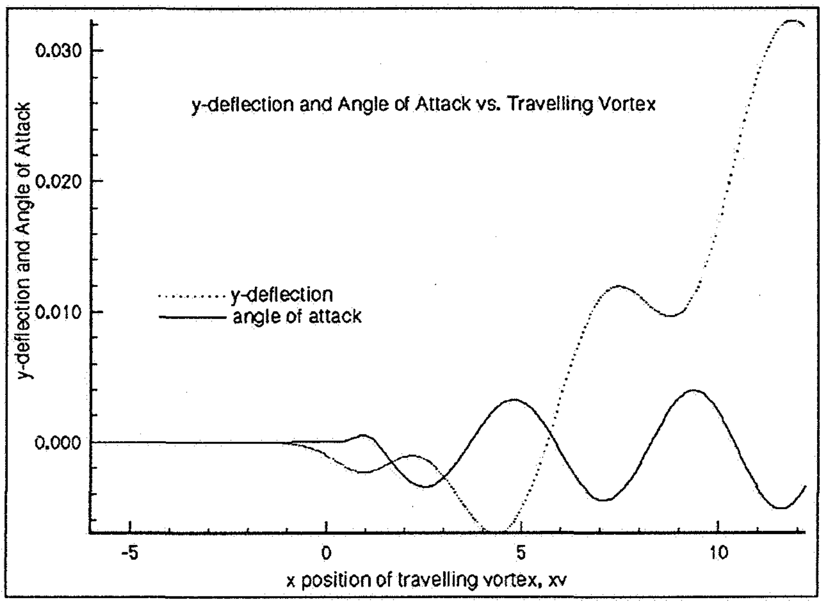

Figure 24: y-deflection and Angle of Attack for a NACA 0012 Airfoil with c.g. at 0.2*c* Interacting with a Vortex, $\Gamma = 0.2$

due to coupling between the pitching and plunging motions when the center of gravity is shifted forward.

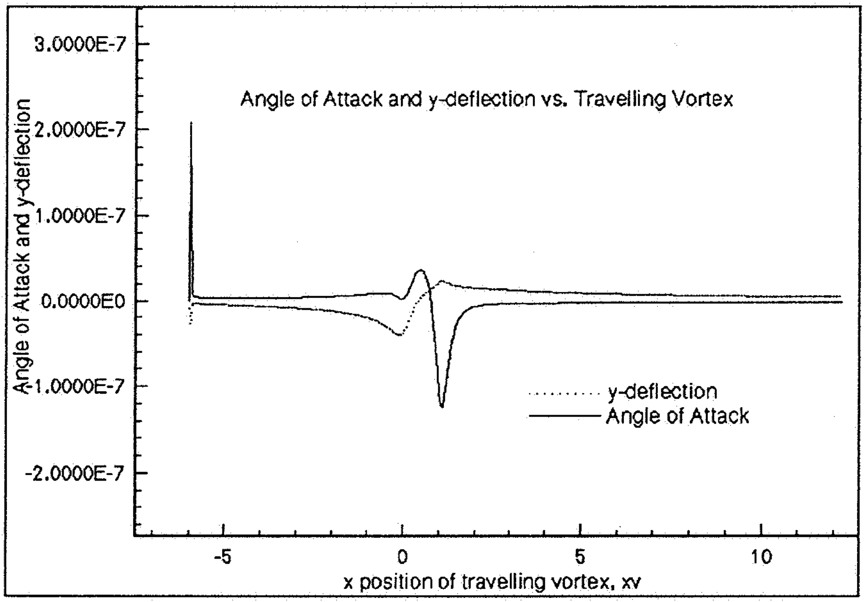

Figure 25: y-deflection and Angle of Attack for a NACA 0012 Airfoil with c.g. at 0.25c Interacting with a Vortex, $\Gamma = 0.2$

Chapter 4 Conclusions

4.1 Constant Potential Panel Method

This panel code successfully models the results of a two-dimensional blade-vortex interaction including aeroelastic movement. These conditions are very topical to the concerns of reducing rotor-noise from helicopters. In order for BVI to be successfully controlled they must first be accurately predicted. Most of the rotor-blade studies that have been performed have treated the blade as rigid in unsteady conditions. This study has shown the necessity of including blade motion in order to calculate useful results.

The current study is limited in a few ways. The flow regimes it models are limited to low speed, incompressible flow. The code can not account for compressibility. Another limitation is that the vortex is represented as a point-vortex which can cause instabilities in the code if it travels too close to the airfoil. Also, the code only allows for one discrete vortex to be included in the system. It is not currently configured to handle more the multiple interactions which will occur in rapid succession in actual flow. Additional vortices could be incorporated relatively easily, however.

4.2 Dynamic Results

The results from the addition of aerodynamic motion to the code show that blade motion is very important, even though the most noticeable changes take place after the vortex has passed the blade. The strength of the vortex is important for reducing the size of the peak values of the parameters studied. vortex strength, however, does not effect the overall trends of the results. A third conclusion is that adding motion to the blade section changes the path that the travelling vortex follows. this would be especially important in situations such as a tandem blade or a rotor-bladed system, where more than one blade interacts with a particular vortex. A last important conclusion to this study is that placement of the center of gravity is also important to motion. Unlike varying vortex strength, center of gravity positions do change the trends of the parameters. Moving the center of gravity slightly forward results in an airfoil that is more statically stable, although the motion takes longer to damp out.

4.3 Further Study

One avenue for further study concerning rotor-noise production would be to test BVI control methods. One method which has been proposed for BVI control is the use of smart structure actuators to change the shape of the airfoil as it moves through each

References

[1] Lee, D. and Smith, C., "Distortion of the Vortex Core During Blade/Vortex Interaction," in *Proceedings of the 19th Fluid Dynamics, Plasma Dynamics and Lasers Conference*, AIAA Paper 87-1243, June 1987.

[2] Wu, J., Sankar, N., and Hsu, T., "Unsteady Aerodynamics of an Airfoil Encountering a Passing Vortex," in *Proceedings of the 23rd Aerospace Sciences Meeting*, AIAA Paper 85-0203, January 1985.

[3] Yao, Z., "Unsteady Aerodynamics of Blade-Blade Interactions," Master's thesis, Arizona State University, December 1993.

[4] Wells, V., "Acoustic and Aeroelastic Considerations in Blade-Vortex Interaction Control." Arizona State University.

[5] Derham, R. C. and Oh, B. K., "The Role of Blade Elasticity in the Prediction of Blade-Vortex Interaction Noise," in *Proceedings of the International Technical Specialists Meeting on Rotorcraft Acoustics and Rotor Fluid Dynamics*, American Helicopter Society and Royal Aeronautical Society, October 1991.

[6] Moran, J., *Theoretical and Computational Aerodynamics*. John Wiley & Sons, Inc., 1984.

[7] Hess, J. and Smith, A., "Calculation of Potential Flow About Arbitrary Bodies," *Prog. Aero. Sci.*, 1967.

[8] Katz, J. and Plotkin, A., *Low-Speed Aerodynamics*. McGraw-Hill, Inc., 1991.

[9] Giesing, J. P., "Nonlinear Two-Dimensional Unsteady Potential Flow with Lift," *Journal of Aircraft*, March 1968.

[10] Kim, M. and Mook, D., "Application of Continuous Vorticity Panels to General Unsteady Incompressible Two-Dimensional Lifting Flows," in *Proceedings of the 23rd Aerospace Sciences Meeting*, AIAA Paper 85-0282, January 1985.

[11] McCroskey, W. and Goorjian, P., "Interactions of Airfoils with Gusts and Concentrated Vortices in Unsteady Transonic Flow," in *Proceedings of the 16th Fluid and Plasma Dynamics Conference*, AIAA Paper 83-1691, July 1983.